arXiv:1601.06646v1 [physics.flu-dyn] 25 Jan 2016

Fast heat transfer calculations in supercritical fluids versus hydrodynamic approach

V. S. Nikolayev,[1,*] A. Dejoan,[2,†] Y. Garrabos,[2] and D. Beysens[1]

[1] *DSM-DRFMC-Service des Basses Températures/ESEME, CEA-Grenoble, France*[‡]
[2] *CNRS-ESEME, Institut de Chimie de la Matière Condensée de Bordeaux, 87, Avenue du Dr. A. Schweitzer, 33608 Pessac Cedex, France*

(Dated: January 26, 2016)

This study investigates the heat transfer in a simple pure fluid whose temperature is slightly above its critical temperature. We propose a efficient numerical method to predict the heat transfer in such fluids when the gravity can be neglected. The method, based on a simplified thermodynamic approach, is compared with direct numerical simulations of the Navier-Stokes and energy equations performed for CO_2 and SF_6. A realistic equation of state is used to describe both fluids. The proposed method agrees with the full hydrodynamic solution and provides a huge gain in computation time. The connection between the purely thermodynamic and hydrodynamic descriptions is also discussed.

I. INTRODUCTION

In fluids near their liquid-gas critical point, the characteristic size of the density fluctuations becomes larger than the characteristic size of the molecular structure. Consequently, the fluid behavior is ruled by fluctuations and not by its particular molecular structure. This implies that most fluids behave similarly near the critical point (like the 3D Ising model). This universality makes the study of near critical fluids very appealing. Due to their very low thermal diffusivity and to their very large thermal expansion and compressibility, the study of heat transfer in such fluids is particularly challenging. When such a fluid is confined in a heated cavity, a very thin hot boundary layer develops and induces a fast expansion that compresses the rest of the fluid. The resulting pressure waves spread at the sound velocity (i.e very rapidly) and adiabatically compress the bulk of the fluid which is therefore homogeneously heated. After several sound wave periods the pressure is already equilibrated and can be assumed to be nearly homogeneous along the cavity. During the initial stage of heating, this process of energy transfer, called "Piston effect" [1, 2], is much more efficient than the usual diffusion scenario. Indeed, if the Piston effect were absent, the bulk of the fluid would remain at the initial temperature.

In the industrial domain, the Piston effect can be used to transfer heat much faster than by conduction. This feature can be readily applied to the development of heat exchangers under microgravity conditions [3, 4] where heat transfer by natural convection is obviously not possible.

While the physical origin of the Piston effect is well understood, the calculations required to represent realistic experimental conditions are difficult because the inherent nonlinear dynamical behavior of such fluids is complicated by the highly non-linear equations of state (EOS) used to describe real near-critical fluids. Two computational approaches have been suggested for confined fluids in absence of convection. In one of them, which we will refer as the "thermodynamic approach" [5], the Piston effect is taken into account by a supplementary term g, introduced in the heat conduction equation as follows,

$$\frac{\partial T}{\partial t} = \frac{1}{\rho c_p}\nabla\cdot(k\nabla T) + g(T), \tag{1}$$

with

$$g(T) = \left(1 - \frac{c_v}{c_p}\right)\left(\frac{\partial T}{\partial p}\right)_\rho \frac{\partial p}{\partial t}, \tag{2}$$

where T is the local fluid temperature, $c_v(c_p)$, the specific heat at constant volume (pressure) per unit mass, ρ the local density and k the thermal conductivity of the fluid. One can note that the term $g(T)$ is only relevant near the critical point where $c_p \gg c_v$.

The fluid motions are neglected and the pressure p, assumed to be homogeneous, is only a function of time t. The pressure p is determined from the fluid mass conservation and computed via the nonlinear expression [5]

$$\frac{\partial p}{\partial t} = -\frac{\int_v (\partial\rho/\partial T)_p \, \partial T/\partial t \, \mathrm{d}v}{\int_v \rho\chi_T \, \mathrm{d}v} \tag{3}$$

where $\chi_T = \rho^{-1}(\partial\rho/\partial p)_T$ is the isothermal compressibility and v the volume of the fluid sample. The resolution of (3) requires an iterative procedure for each time step. This consists in calculating the temperature *in the whole fluid volume* using Eqs. (1-2) for some trial value of p (and thus $\partial p/\partial t$) and determining the other thermodynamic parameters (ρ, χ_T, ...) by an EOS

$$\Lambda(p, \rho, T) = 0. \tag{4}$$

Subsequent computation of the *volume* integrals in Eq.(3) gives a new value of $\partial p/\partial t$ from which the pressure p is corrected. The correction step is repeated until

*email:vnikolayev@cea.fr
†Present address: Aeronautics Department, Imperial College, Prince Consort Road, South Kensington, London, England, SW7 2BY, United Kingdom
‡Mailing address: CEA-ESEME, Institut de Chimie de la Matière Condensée de Bordeaux, 87, Avenue du Dr. A. Schweitzer, 33608 Pessac Cedex, France

convergence. This approach has been extensively used by several groups [6, 7] in one-dimensional (1D) calculation in conjunction with the restricted cubic EOS [8] and the finite difference numerical method. However, its extension to higher dimensions induces a large computational effort. First, it requires a sophisticated programming and, second, the computer resources rise steeply because the thermodynamic variables have to be evaluated at each grid point of the computational domain by means of the iterative procedure to solve Eq. (3).

Teams with expertise in theoretical hydrodynamics have developed a rigorous hydrodynamic approach [1] in which the Navier-Stokes and energy equations are coupled with the EOS. This set of equations has been solved analytically in 1D by asymptotic matching techniques [9] and also by direct numerical simulation (DNS) [10] via the finite volume method [11] both in 1D and 2D. For the sake of simplicity, the van der Waals EOS has been used in all these works. Although this simple EOS provides satisfactory qualitative results, accuracy can only be ensured by using a realistic EOS. However, as shown in the present study, inserting a realistic EOS into the hydrodynamic equations leads to a much more difficult computational task, which involves prohibitively large calculation times. For instance, to reach the final steady state in one of the 1D runs carried out for the cubic EOS in the present study, one requires about two months on a 800 MHz PC.

The purpose of this article is twofold. We first formulate an approximate method which is both simple and rapid (e.g., the same calculation cited above required only 20s !) and then compare it with the DNS formalism. Second, since this work is the first one to use a realistic EOS for the DNS, we describe in detail the hydrodynamic approach for the near-critical fluids with a general EOS. We expect that this complete and unified description may be useful for the scientific community, as the hydrodynamic method is dispersed over many (some of them not easily accessible) publications.

The article is organized as follows. In Sec. II we describe the fast calculation method. Sec. III presents the hydrodynamic approach. Sec. IV deals with the comparison between both approaches. The conclusions are given in Sec. V.

II. FAST CALCULATION METHOD

The method is based on the thermodynamic approach, i.e. on the energy equation (1). However, a different pressure equation will be used instead of Eq. (3). While the latter equation integrates over the fluid *volume*, we are looking for a pressure equation that integrates only over the *boundaries* of the fluid domain. Such an equation would accelerate the iterative procedure. However, its advantage would not be decisive without an appropriate numerical method for Eq. (1) that should only require computation of the thermodynamic variables at the boundaries. Such a numerical method is called Boundary Element Method (BEM) and is broadly used in heat transfer problems. The BEM is expounded in Appendix A.

Several simplifications have to be introduced before presenting the formulation of the energy and pressure equations used in the present method. As stated in the introduction, we are mainly interested in the description of the early stages of the heating, i.e. on times of the order of the Piston effect time scale [12]. In this regime, the thermodynamic quantities $c_p, c_v, k, \ldots$ are constant in the bulk of the fluid and only vary in the very thin hot and cold boundary layers. Thus, the following assumptions can be made:

(i) The spatially varying parameters (c_p, c_v, k, etc.) in Eq. (1) can be replaced by the spatially homogeneous time dependent values which will be denoted hereafter by an over-bar (e.g. $\bar{c}_p$). These values are calculated with the EOS using density $\langle\rho\rangle$ (where the brackets indicate the spatial average) and the pressure $p = p(t)$. We note that the density $\langle\rho\rangle$ is constant as the system is closed.

This assumption is equivalent to the statement that all these quantities should be calculated using the temperature value $\bar{T} = \bar{T}(t)$ obtained from the EOS for the pressure p and the density $\langle\rho\rangle$. The quantities calculated in such a way correspond to the over-bar variables mentioned above . In general, for a thermodynamic quantity X, $\bar{X} \neq \langle X\rangle$.

(ii) During the system evolution, the thermodynamic quantities are supposed not to vary sharply in time.

(iii) The initial temperature T_0 is uniform.

The assumption (iii) is made for simplicity and can be relaxed if necessary. However, the assumptions (i) and (ii) are essential for this approach.

In the following section we formulate the energy and pressure equations that govern the kinetics of the supercritical fluid in a reduced gravity environment.

A. Energy equation

Using the assumption (i) and the constancy of $\langle\rho\rangle$, one can write

$$\mathrm{d}p = \overline{(\partial p/\partial T)}_\rho \mathrm{d}\bar{T} \tag{5}$$

so that the term (2) reduces to

$$\bar{g}(\bar{T}) = \left(1 - \frac{\bar{c}_v}{\bar{c}_p}\right)\frac{\mathrm{d}\bar{T}}{\mathrm{d}t}, \tag{6}$$

and Eq. (1) can be reduced to the equation

$$\frac{\partial\psi}{\partial t} = \bar{D}\nabla^2\psi. \tag{7}$$

The thermal diffusion coefficient $\bar{D} = \bar{k}/\langle\rho\rangle\bar{c}_p$ depends on $\bar{T}$ i.e. on time t only, and

$$\psi(\vec{x}, t) = T(\vec{x}, t) - T_0 - E(\bar{T}). \tag{8}$$

with $\vec{x}$ the position vector and

$$E(\bar{T}) = \int_{T_0}^{\bar{T}} \left(1 - \frac{\bar{c}_v}{\bar{c}_p}\right) \mathrm{d}\bar{T}. \tag{9}$$

The initial condition is $\psi|_{t=0} = 0$ because according to the assumption (iii),

$$\bar{T}|_{t=0} = T_0. \tag{10}$$

Finally, a known dependence of $\bar{D} = D_d\, f(\bar{T})$, where D_d is a dimensional constant and f is a non-dimensional function, allows the time t to be replaced by a new independent variable τ defined by the equation

$$\frac{\mathrm{d}\tau}{\mathrm{d}t} = f(\bar{T}), \tag{11}$$

whose initial condition can be imposed as $\tau|_{t=0} = 0$. Since $\bar{T}$ is a function of t only, this initial value problem is fully defined. The substitution of Eq. (11) into Eq. (7) results in the linear diffusion problem with the constant diffusion coefficient D_d

$$\begin{aligned} \frac{\partial \psi}{\partial \tau} &= D_d \nabla^2 \psi, \\ \psi|_{\tau=0} &= 0. \end{aligned} \tag{12}$$

It can be solved with BEM as shown in Appendix A.

Usually, the "temperature step" boundary condition has been applied for 1D problems. This heating process corresponds to a fluid cell, initially at a uniform temperature, which is submitted to a sudden increase of temperature at one of its boundaries, while the other is kept at the initial temperature (Dirichlet boundary conditions). This heating condition is physically unrealistic because the initial value for the heat flux at the heated boundary is infinite. Instead, in this work we use Neumann-Dirichlet boundary conditions: a heat flux q_{in} is imposed at one of the boundaries, while the initial temperature T_0 is maintained at the other boundary.

B. Boundary form of the pressure equation

Let us begin by writing the linearized relationship, valid under the assumption (ii):

$$\delta\rho = \left(\frac{\partial \rho}{\partial s}\right)_p \delta s + \left(\frac{\partial \rho}{\partial p}\right)_s \delta p, \tag{13}$$

where s is the fluid entropy per unit mass and δ stands for the variation of the thermodynamic quantity during the time interval δt. From mass conservation it follows $\langle \delta\rho \rangle = 0$, and, from the pressure homogeneity that $\langle \delta p \rangle = \delta p$.

By averaging Eq. (13) one obtains

$$\langle \left(\frac{\partial \rho}{\partial s}\right)_p \delta s \rangle + \langle \left(\frac{\partial \rho}{\partial p}\right)_s \rangle\, \delta p = 0. \tag{14}$$

The use of appropriate thermodynamic relationships leads to

$$\delta p = \frac{\left\langle \frac{\chi_T}{c_p} T \left(\frac{\partial p}{\partial T}\right)_\rho \rho \delta s \right\rangle}{\left\langle \frac{\chi_T}{c_p} \rho c_v \right\rangle}. \tag{15}$$

In order to use the second law of thermodynamics

$$\langle \rho \delta s \rangle = \frac{\delta Q}{v\bar{T}}, \tag{16}$$

where δQ is the total change of the amount of heat of the fluid, one needs to separate out the averages of the form $\langle YZ \rangle$ in Eq. (15). Under the assumption that Y (or Z) does not vary sharply over the fluid volume, the following approximation holds (see Appendix C):

$$\langle YZ \rangle \approx \langle Y \rangle \langle Z \rangle. \tag{17}$$

Among the quantities that appear in Eq. (15), only χ_T and c_p vary sharply near the critical point and could thus vary strongly across the fluid volume. However, only their ratio, which remains constant near the critical point, enters Eq. (15). Hence, the average of this ratio as well as the remainder averages of slowly varying quantities can be separated. By using the expression for the total heat change rate

$$\frac{\delta Q}{\delta t} = \int_A k \frac{\partial T}{\partial \vec{n}} \mathrm{d}A, \tag{18}$$

where the r.h.s. is simply the integrated heat flux supplied to the fluid through its boundary A (with $\vec{n}$ the external normal vector to it), one gets to the final expression

$$\frac{\mathrm{d}\bar{T}}{\mathrm{d}t} = \frac{1}{\langle \rho \rangle v c_v} \int_A k \frac{\partial T}{\partial \vec{n}} \mathrm{d}A. \tag{19}$$

In the fast calculation method, Eq. (19) plays the role of the pressure equation (3). Equation (19) is both substituted directly into Eq. (6) and solved to get the temperature $\bar{T}$ using the initial condition (10). The obtained value for $\bar{T}$ is used to solve Eq. (11) and to calculate all the fluid properties. Note that $\bar{T}$ should not be confused with T from Eqs. (18, 19). The spatially varying fluid temperature T has to be calculated with Eqs. (8,12).

Substituting $\bar{T}$ by $\langle T \rangle$, Eq. (19) coincides with the result of Onuki and Ferrell [2] which was derived by a different way. Eq. (19), written in terms of $\langle T \rangle$, was employed recently [13, 14] to simulate the gravitational convection in 2D by the finite difference method. However, the finite difference numerical method is not the most efficient for the computation of heat transfer problems.

III. HYDRODYNAMIC APPROACH

Analytical analysis as well as direct simulations were carried out in previous works. Bailly and Zappoli [15]

have developed a complete hydrodynamic theory of density relaxation after a temperature step at the boundary of a cell filled with a nearly supercritical fluid in microgravity conditions. In [15] they describe the different stages of the fluid relaxation towards its complete thermodynamic equilibrium, covering the acoustic, Piston effect and heat diffusion time scale. The analytical approach leans on the matched asymptotic expansions to solve the 1D Navier-Stokes equations for a viscous, low-heat-diffusing, near-critical van der Waals fluid (see [9] and [15]). The DNS of the Navier-Stokes equations were performed in 1D and 2D geometries. Some of them take into account gravity effects, as for example, the interaction of a near-critical thermal plume with a thermostated boundary [16]. Numerical results are also available on thermo-vibrational mechanisms [17].

To date the hydrodynamic approach has been solved for the classical, van der Waals, EOS. This EOS allows a considerable reduction in computational time when compared to the restricted cubic EOS. However, it does not provide a correct description of the real fluids. In particular, it fails to predict the critical exponents for the divergence laws of the thermodynamic properties. In the present work we use a more realistic cubic EOS to describe the fluid behavior in the near-critical region. Hereafter, we describe the methodology suitable for a general EOS.

A. Problem statement

The hydrodynamic description leads to the following set of equations

$$\frac{\mathrm{d}\rho}{\mathrm{d}t} + \rho\nabla\cdot\vec{u} = 0, \tag{20}$$

$$\rho\frac{\mathrm{d}\vec{u}}{\mathrm{d}t} = -\nabla p + \mu\nabla^2\vec{u}, \tag{21}$$

$$\rho\frac{\mathrm{d}e}{\mathrm{d}t} = \nabla\cdot(k\nabla T) - p\nabla\cdot\vec{u} + \Phi, \tag{22}$$

where e is internal energy per unit mass, $\vec{u} = (u_1, u_2, u_3)$ is the fluid velocity at the point $\vec{x} = (x_1, x_2, x_3)$,

$$\Phi = \mu\sum_{i,j}\left(\frac{\partial u_i}{\partial x_j}\frac{\partial u_j}{\partial x_i} + \frac{\partial u_i}{\partial x_j}\frac{\partial u_i}{\partial x_j} - \frac{2}{3}\frac{\partial u_i}{\partial x_i}\frac{\partial u_j}{\partial x_j}\right)$$

is the dissipation function due to the shear viscosity μ (the bulk viscosity is neglected). The operator $\mathrm{d}/\mathrm{d}t$ is defined as

$$\frac{\mathrm{d}}{\mathrm{d}t} = \frac{\partial}{\partial t} + \vec{u}\cdot\nabla. \tag{23}$$

The set of equations (20,21,22) is closed by adding the EOS (4).

B. c_v-formulation

In the DNS, the energy equation (22) is re-written in terms of temperature T. This is achieved by expressing the internal energy as a function of density and temperature so that one can make use of the well known relation

$$\frac{\mathrm{d}e}{\mathrm{d}t} = \frac{1}{\rho^2}\left[p - T\left(\frac{\partial p}{\partial T}\right)_\rho\right]\frac{\mathrm{d}\rho}{\mathrm{d}t} + c_v\frac{\mathrm{d}T}{\mathrm{d}t}. \tag{24}$$

Then, by substituting the Eqs. (20) and (22) into Eq. (24) one obtains:

$$\rho c_v\frac{\mathrm{d}T}{\mathrm{d}t} = \nabla\cdot(k\nabla T) - T\left(\frac{\partial p}{\partial T}\right)_\rho\nabla\cdot\vec{u} + \Phi. \tag{25}$$

Note that Eq. (25) involves c_v and not c_p as in the thermodynamic Eq. (1). The "c_v-formulation" is preferred to the "c_p-formulation" because the much weaker near-critical divergence of c_v (in comparison to c_p) allows c_v to be assumed constant.

The boundary conditions for the Navier-Stokes equations are $\vec{u} = 0$ at the walls. The initial conditions are given by $\vec{u}(t=0) = 0$. For the energy equation (25) the boundary and initial conditions are identical to those applied in the energy equation (1) (cf. Sec. II). The values of the physical parameters used in the simulations are discussed in Appendix B.

C. Acoustic filtering

Heat transfer in supercritical fluid involves three characteristic time scales [12, 18]: the acoustic time scale defined by $t_a = L/c_0$ (where c_0 is the sound velocity and L is the cell size), the diffusion time scale $t_D = L^2/D$ (D being the thermal diffusivity) and the Piston Effect time scale defined by $t_{PE} = L^2/[D(c_p/c_v - 1)^2]$, with $t_a \ll t_{PE} < t_D$. The present study is mainly concerned with time of the same order as the Piston effect time scale so that a fine description of the acoustic phenomena is not needed. This suggests that one can filter out the acoustic motions of the set of Eqs. (4,20,21,25) and retain only their integrated effects without altering the physics of our problem. The removal of the acoustic motions is achieved by applying the acoustic filtering method [19] which is broadly used in the computation of the low Mach number compressible Navier-Stokes equations because it avoids numerical instabilities when time steps, $\Delta t >> t_a$, are used in the simulations. The following presents the main points of the acoustic filtering method.

The equation of momentum is first rewritten by choosing the sound velocity c_0 as the reference velocity scale and L/u_0 as the reference time scale (here u_0 is the characteristic velocity of large scale fluid motions, in our case $u_0 = L/t_{PE}$). Using this time and velocity scale the Mach number $\mathrm{Ma} = u_0/c_0$ appears in the non-

dimensional momentum equation as follows,

$$\rho\left[\frac{\partial\vec{u}}{\partial t}+\mathrm{Ma}^{-1}(\vec{u}\cdot\nabla)\vec{u}\right]=-\frac{\mathrm{Ma}^{-1}p_c}{c_0^2\rho_c}\nabla p+\frac{1}{\mathrm{Re}}\nabla^2\vec{u}, \tag{26}$$

where $\mathrm{Re}=\rho_c u_0 L/\mu$ is the Reynolds number and the density and pressure are non-dimensionalized by the critical density ρ_c and critical pressure p_c taken as the reference values. For small Mach numbers, one can express the fluid variables as series of Ma,

$$\vec{u}=\mathrm{Ma}[\vec{u}^{(0)}+\mathrm{Ma}^2\vec{u}^{(1)}+o(\mathrm{Ma}^2)], \tag{27}$$

$$p=p^{(0)}+\mathrm{Ma}^2p^{(1)}+o(\mathrm{Ma}^2), \tag{28}$$

While $\vec{u}$ in the l.h.s. of Eq. (27) is non-dimensionalized with c_0, the term in the square brackets defines the velocity non-dimensionalized with u_0. This explains the factor Ma in Eq. (27). The density and temperature are expanded like p in Eq. (28). By substituting the series (27, 28) into Eq. (26) and neglecting the terms of order $O(\mathrm{Ma})$, one obtains $\nabla p^{(0)}=0$, which means that $p^{(0)}$ depends on time only. By retaining $O(\mathrm{Ma})$ terms in Eqs. (20,25,26) and $O(1)$ terms in the EOS (4), one obtains the final (dimensional) form for the governing equations:

$$\frac{\mathrm{d}\rho^{(0)}}{\mathrm{d}t}=-\rho^{(0)}\nabla\cdot\vec{u}^{(0)}, \tag{29}$$

$$\rho^{(0)}\frac{\mathrm{d}\vec{u}^{(0)}}{\mathrm{d}t}=-\nabla p^{(1)}+\mu\nabla^2\vec{u}^{(0)}, \tag{30}$$

$$\rho^{(0)}c_v^{(0)}\frac{\mathrm{d}T^{(0)}}{\mathrm{d}t}=-T^{(0)}\left(\frac{\partial p}{\partial T}\right)_\rho\nabla\cdot\vec{u}^{(0)}+\nabla\cdot(k\nabla T^{(0)}), \tag{31}$$

$$\Lambda(p^{(0)},\rho^{(0)},T^{(0)})=0, \tag{32}$$

where $(p_c/c_0^2\rho_c)p^{(1)}$ is replaced by $p^{(1)}$ for the sake of compactness. The pressure term $p^{(1)}$ has to be interpreted as the dynamic pressure that makes the velocity field satisfy the continuity equation (29). This term reflects the contribution of the acoustic waves averaged over several wave periods to the total pressure field. One notes that the velocity scale c_0 is not present any more in Eqs. (29-32) which was the main purpose of the acoustic filtering.

The assessment of $p^{(0)}$ requires one more equation to close the set (29-32). This additional equation expresses the mass conservation:

$$\frac{1}{v}\int_v\rho^{(0)}dv=\langle\rho\rangle, \tag{33}$$

where $\langle\rho\rangle$ is a known constant.

In the following, the superscript (0) is dropped to conform to the notation of Sec. II.

D. Numerical procedure

For the time integration, the first order Euler scheme is used. Equations (29-31) are solved by the iterative SIMPLER algorithm and by applying the Finite Volume Method (FVM, see Appendix D) on each grid cell of the 1D cell. Near the walls the mesh is refined to properly resolve the very thin thermal boundary layers.

In the present work the thermodynamics variables are determined using the parametric EOS [8]. This uses two parameters r and θ which both depend on temperature T and density ρ. Therefore, one needs to solve two equations

$$\begin{aligned}\Lambda_1(r_i,\theta_i,T_i)&=0\\ \Lambda_2(r_i,\theta_i,p)&=0\end{aligned} \tag{34}$$

instead of one Eq. (4) for each volume element i and time step.

The whole numerical procedure consists in solving by the Newton-Raphson method, at each time step, a set of equations that includes Eqs. (34), written for each volume element and Eq. (33). This makes a system of $2N+1$ equations to resolve, N being the total number of the volume elements. The local temperature T_i is given by the resolution of Eqs. (29-31) at each iteration of the SIMPLER algorithm for each time step, as described in Appendix D. For each value T_i the $2N+1$ (r_i,θ_i,p) variables are computed via the system (34).

IV. RESULTS AND DISCUSSION

A brief analysis comparing the c_p and c_v formulations (1) and (31) of the energy equation allows us to gain more insight into the relation between the two approaches. Formally, Eq.(1) and Eq.(31) become equivalent if the advection term

$$(\vec{u}\cdot\nabla)T \tag{35}$$

is added to l.h.s. of Eq. (1). However, the equivalence of the two forms under which the pressure work appears (see second term of the l.h.s of Eq.(1) and Eq.(31)) is not trivial and deserves to be detailed. At the early stage of the heating ($t<t_{PE}$) the velocity at the front of the cold boundary layer being very small, the velocity can be assumed to decrease linearly in the bulk cell as $\partial u/\partial x\simeq -u_{max}/L$, where u_{max} is the maximum velocity located at the front of the hot boundary layer and x the distance from the hot wall to the cold wall. The rate of temperature increase due to the pressure contribution in Eq. (31) can thus be written as follows,

$$-\frac{T}{\rho c_v}\left(\frac{\partial p}{\partial T}\right)_\rho\nabla\cdot\vec{u}=\frac{T}{\rho c_v}\left(\frac{\partial p}{\partial T}\right)_\rho\frac{u_{max}}{L} \tag{36}$$

By using the expression [12],

$$u_{max}=\frac{1}{T}\left(\frac{\partial T}{\partial p}\right)_\rho\frac{\delta Q}{A\delta t}, \tag{37}$$

and Eqs. (18,19) one concludes that the term (36) is equivalent to (6) near the critical point where $c_p\gg c_v$.

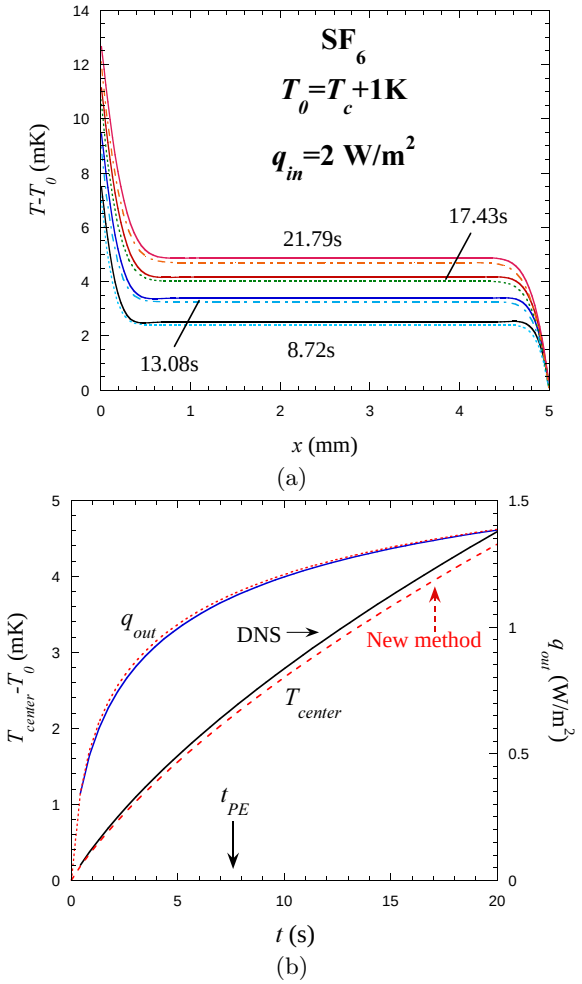

FIG. 1: Comparison of two approaches for SF_6 at 1K above T_c (reduced temperature $3.1 \cdot 10^{-3}$), $q_{in} = 2$ W/m^2 and $\langle \rho \rangle = \rho_c$. Solid curves are the DNS results and the dotted curves are the new method results. (a) Spatial variation of the temperature at different times. (b) Time evolution of the temperature at the cell center and of the flux at the exit of the cell. The value of $t_{PE} = 7.73$ s obtained with our EOS is shown by an arrow.

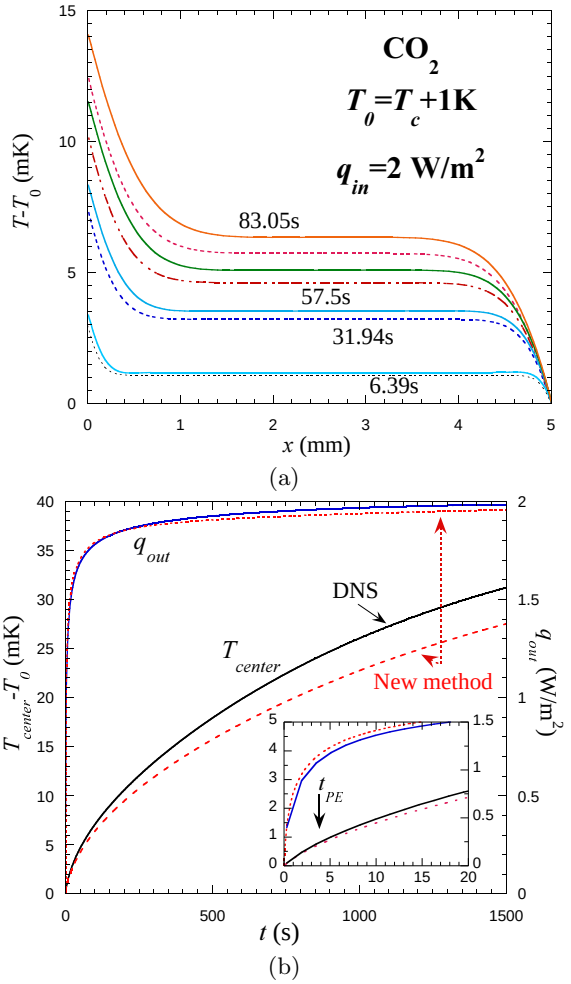

FIG. 2: Comparison of the two approaches for CO_2 at 1K above T_c (reduced temperature $3.3 \cdot 10^{-3}$), $q_{in} = 2$ W/m^2 and $\langle \rho \rangle = \rho_c$. Solid curves are the DNS results and the dotted curves are the new method results. (a) Spatial variation of the temperature at different times. (b) Time evolution of the temperature at the cell center and of the flux at the exit of the cell. The value of $t_{PE} = 3.45$ s obtained with our EOS is shown by an arrow in the insert that presents the short time evolution.

One can note that in the hydrodynamic approach, the pressure work is directly related to the mass transfer from the hot boundary layer to the bulk fluid via the gradient velocity. It is then very important to asses properly the effect of the velocity field in order to compare the fast calculation and hydrodynamic methods. The above analysis has shown that the expressions of the pressure work is equivalent for both methods. Hence, the remaining potential interaction between the velocity and energy fields can manifest itself only through the advection term (35). This term is only relevant when, at the same spot of the fluid, both the fluid velocity and the temperature gradient are large. At the small times, $t < t_{PE}$, the temperature gradients are confined very near the wall where the velocity remains small [18]. Later on, the velocity maximum shifts to the center of the cell where the temperature gradient is small. At very large times, $t > t_D$, the Piston effect is not efficient and the velocity tends to zero. We thus do not expect a strong influence of the advection effects on the temperature field. This will be confirmed by the results presented below. Note that the advection term cannot be neglected when the flux distribution over the heater surface is highly inhomogeneous. Hot jets [26] can be generated in this case.

The calculations have been performed for two fluids, CO_2 and SF_6, confined in a cell of length $L = 5$mm. The initial temperatures 1K and 5K above the critical point have been considered for CO_2. The computations related to SF_6 concern only the initial temperature 1K above the critical point. The cell boundary situated at $x = 0$ has

been submitted to the constant heat flux $q_{in} = 2\mathrm{W/m^2}$ (for $T_0 = T_c{+}1\mathrm{K}$) and $q_{in} = 9.5\mathrm{W/m^2}$ (for $T_0 = T_c{+}5\mathrm{K}$) and the opposite boundary has been maintained at the constant temperature $T(x = L) = T_0$.

The time evolution of the temperature profiles and the temperature at the cell center $T_{center} = T(x = L/2)$ as well as the heat flux $q_{out} = -k\frac{\partial T(x=L)}{\partial x}$ are compared and analyzed. In the case of CO_2, the time evolution covers not only the Piston effect time scale t_{PE} but also the large diffusion time scale.

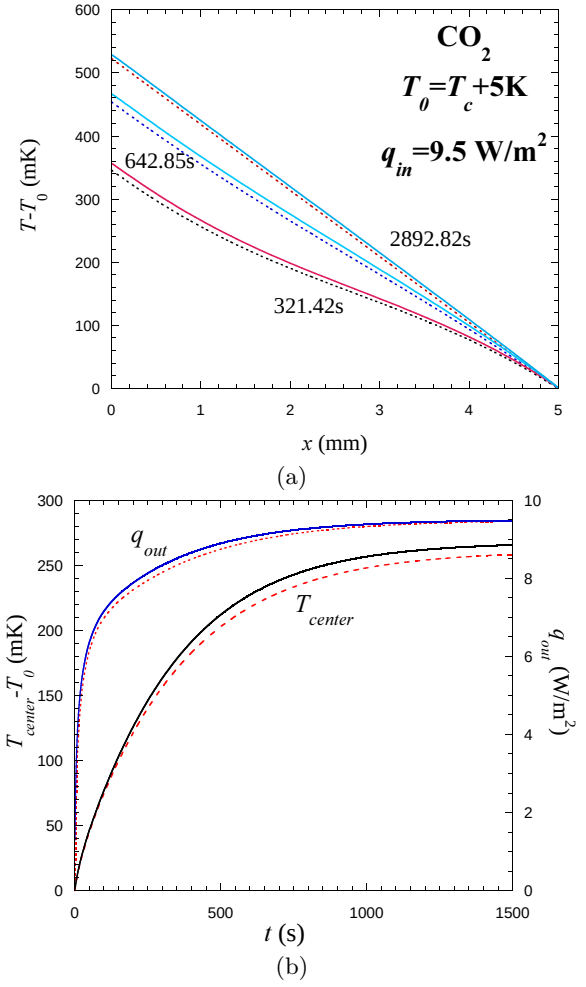

FIG. 3: Comparison of two approaches for CO_2 at 5K above the critical temperature (reduced temperature $1.6 \cdot 10^{-2}$), $q_{in} = 9.5\ \mathrm{W/m^2}$ and $\langle\rho\rangle = \rho_c$. Solid curves are the DNS results and the dotted curves are the new method results. According to our EOS, $t_{PE} = 25.67$ s. (a) Spatial variation of the temperature at different times. (b) Time evolution of the temperature at the cell center and of the flux at the exit of the cell.

The set of Figs. 1, 2, and 3 exhibit a very good qualitative agreement between the DNS and the fast calculation results. The thin boundary layers and the homogeneous enhancement of the temperature in the center cell are very well predicted. The quantitative comparison sets out two behaviors. On one hand, the flux q_{out} appears to fit very well with the DNS over the full time evolution, at the time scale t_{PE} as well at the time scale t_D, see Figs. 2b, 3b. On the other hand, the temperature at the cell center T_{center} tends to be lower than the DNS data. This discrepancy increases with time and is larger when the temperature is closer to the critical temperature (see Fig. 2b and Fig. 3b). Both behaviors can be explained by considering how the thermal conductivity k is estimated in each method. In the hydrodynamic approach k is determined locally, whereas the fast calculation uses the spatial average value of k. Thus, keeping in mind that the thermal conductivity diverges when approaching the critical point, the increment in temperature near the heating surface tends to be smaller in the new method than in the DNS (see Fig. 2a). At the opposite surface the temperature is fixed at the initial temperature and is closest to the bulk temperature so that the effect of averaging k is less influent in this region. One can note that the thermal diffusivity can be computed locally in the fast calculation method by applying the Kirchhoff substitution of the dependent variable ψ (defined by Eq. (8)) by $\phi = \int_0^{\psi} k(\psi)\mathrm{d}\psi$.

A physical interpretation of the temperature $\bar{T}$, which was formally introduced in Sec. II, can now be given. Indeed, since in the fluid bulk (i.e., arround the center of the cell) $\frac{\partial T}{\partial x} = 0$ at $t < t_{PE}$, according to Eq. (1) we have $\partial T_{center}/\partial t = \bar{g}(\bar{T})$. As near the critical point $c_p \gg c_v$, Eq. (6) provides $\bar{g}(\bar{T}) \approx \partial\bar{T}/\partial t$. Finally, one can conclude that $\bar{T} \approx T_{center}$. In other words, $\bar{T}$ can be considered as the bulk temperature.

Aa a further remark, we note that for 1D the Eq. (A1) could have been solved analytically by series expansion. Nevertheless, we prefer the use of the BEM for its generality and its possible extension to higher dimensions. We note that in 2D and 3D the BEM remains advantageous in resolving linearized problems when compared to other numerical methods. Its success is based on several factors. One of them is its numerical stability: the numerical solution of the integral equations is much more stable than that of the differential equations and allows the use of larger time steps. Another advantage consists in the possibility of determining analytically the BEM coefficients, Eqs. (A6, A7). For 2D configurations, the diagonal coefficients G_{FF} and H_{FF} (which have the largest absolute value and thus are the most relevant) can be calculated analytically. The semi-analytical integration can be used for the remaining coefficients [22, 23].

V. CONCLUSIONS

In this work we propose a thermodynamic method for describing the heat transfer in supercritical fluids in absence of gravity effects. The method has been compared with the solution of the full hydrodynamic equations, showing an excellent agreement. In general, a thermodynamic approach leans on the possibility of expressing

the pressure work independently of the velocity field. If so, the transfer of momentum does not need to be considered, allowing a large reduction in computational time. As an example, in calculations carried out for CO_2 and SF_6, the present thermodynamic method within minutes provided the complete evolution of the heat transfer process, while the direct numerical simulation of the full hydrodynamic equations required weeks of CPU time.

Compared with previous thermodynamic methods [5], the fast calculation method presented here does not require the evaluation of the variables at each cell of the computation domain. This fact ensures a much better performance. Moreover, the proposed method offers the possibility to explicitly include the thermal behaviour of the material vessel containing the fluid by taking into account the heat conduction along the solid walls, see Ref. [4].

The direct numerical simulation of the flow has been used to analyze the validity of the method proposed here. The accuracy of the latter approach is explained by the fact that the advection of energy remains negligible.

For the sake of completeness, we have also presented a detailed description of the hydrodynamic approach. While it has been used for about a decade, some parts of its description for a general equation of state are either dispersed over many literature sources or not published at all in the accessible literature.

Concerning the future development of the present research, we plan to extend the fast calculation method to two- and three-dimensional problems. Finally, we intend to use this method to investigate the heat transfer in two-phase fluids.

Acknowledgments

This work was partially supported by the CNES. We thank Carole Lecoutre for her help with the code launching. A. D. acknowledges Jalil Ouazzani for the helpful discussions on the numerical method used in the hydrodynamic approach.

Appendix A: BEM for the diffusion equation

In this Appendix we use the traditional notation, so that D and t correspond to D_d and τ of Eq. (12). It can be shown [21] that the linear diffusion problem

$$\frac{\partial \psi}{\partial t} = D\nabla^2\psi \qquad \psi|_{t=0} = 0 \tag{A1}$$

with the constant thermal diffusion coefficient D is equivalent to the boundary integral equation

$$D\int_0^t \mathrm{d}t' \int_A \left[G(\vec{x}-\vec{x'},t-t')\frac{\partial_{x'}\psi(\vec{x'},t')}{\partial \vec{n}} - \psi(\vec{x'},t')\frac{\partial_{x'}G(\vec{x}-\vec{x'},t-t')}{\partial \vec{n}} \right] \mathrm{d}_{x'}A = \frac{1}{2}\psi(\vec{x},t). \tag{A2}$$

The integration is performed over the surface A of the fluid volume v, $\vec{x} \in A$. The outward unit normal to A is $\vec{n}$. The Green function G for the infinite space for the equation adjoint to Eq. (A1) reads

$$G(\vec{x},t) = (4\pi D t)^{-d/2} \exp\left(-\frac{|\vec{x}|^2}{4Dt}\right), \tag{A3}$$

where d is the spatial dimensionality of the problem (A1).

Only the 1D case with the space variable $x \in (0, L)$ is considered below, the 2D counterpart being described elsewhere [22, 23]. For $d = 1$, A degenerates into two points, and Eq. (A2) reduces to two equations

$$2D\int_0^t \mathrm{d}t' \left[G(x-x',t-t')\frac{\partial \psi}{\partial x'} - \psi(x',t')\frac{\partial G(x-x',t-t')}{\partial x'} \right]\Bigg|_{x'=0}^{x'=L} = \psi(x,t) \tag{A4}$$

written for $x = 0, L$. A variety of numerical methods can be applied to solve Eqs. (A4). The simplest way is to present the integral over $(0, t)$ as a sum of the integrals over (t_{f-1}, t_f), $f = 1..F$ with $t_0 = 0$ and $t_F = t$ and assume a constant values $\psi_f = \psi(t_f)$ and $\psi'_f = \partial\psi(t_f)/\partial x$ over each of these intervals. Eqs. (A4) will reduce then to the set of $2F_m$ (t_{F_m} is the maximum desired calculation time) linear equations

$$\sum_{f=1}^{F} [\psi_f(0)H_{Ff}(x) - \psi_f(L)H_{Ff}(x-L) - \psi'_f(0)G_{Ff}(x) + \psi'_f(L)G_{Ff}(x-L)] = \psi_{Fi}/2, \quad x = 0, L;\ F = 1, F_m \tag{A5}$$

for $4F_m$ variables ψ_f, $\psi'_f(0, L)$, $2F_m$ of them being defined by the boundary conditions. The coefficients in these equations can be calculated analytically:

$$G_{Ff}(x) = D\int_{t_{f-1}}^{t_f} G(x, t_F - t')\mathrm{d}t' = \frac{|x|}{2}\left[\mathrm{erfc}(\sqrt{u}) - \frac{\exp(-u)}{\sqrt{u\pi}}\right]\Bigg|_{\frac{x^2}{4D(t_F-t_f)}}^{\frac{x^2}{4D(t_F-t_{f-1})}} \tag{A6}$$

and

$$H_{Ff}(x) = -D\int_{t_{f-1}}^{t_f} \frac{\partial G(x, t_F - t')}{\partial x}\mathrm{d}t' = -\frac{\mathrm{sign}(x)}{2}\mathrm{erfc}(\sqrt{u})\Big|_{\frac{x^2}{4D(t_F-t_f)}}^{\frac{x^2}{4D(t_F-t_{f-1})}}, \tag{A7}$$

where

$$\mathrm{erfc}(x) = \int_x^\infty \exp(-u^2)\mathrm{d}u,$$

is the complementary error function and

$$\mathrm{sign}(x) = \begin{cases} 1, & x > 0, \\ -1, & x < 0. \end{cases}$$

One needs to mention that the case $x = 0$ is special: $H_{Ff}(0) = 0$ for all f and F and

$$G_{Ff}(0) = \sqrt{D_0/\pi}(\sqrt{t_F - t_{f-1}} - \sqrt{t_F - t_f}\,).$$

The set of linear equations (A5) can be solved by any appropriate method, e.g. by the Gauss elimination.

Appendix B: The fluid properties

The thermal conductivity k is deduced from the thermal diffusivity

$$D = D_1\left(\frac{T - T_c}{T_c}\right)^{\varphi_1} + D_2\left(\frac{T - T_c}{T_c}\right)^{\varphi_2} \tag{B1}$$

and the constant pressure specific heat at critical density ρ_c, $k = D\rho_c c_p|_{\rho_c}$. Coefficients values for CO_2 are:

$D_1 = 5.89184 \times 10^{-8}$ m^2/s, $D_2 = 7.98068 \times 10^{-7}$ m^2/s, $\varphi_1 = 0.67$ and $\varphi_2 = 1.24$.

Coefficients values for SF_6 are:

$D_1 = 6.457 \times 10^{-7}$ m^2/s, $D_2 = 0$, $\varphi_1 = 0.877$ and $\varphi_2 = 0$.

The specific heat at constant pressure is calculated by using the thermodynamic relationship

$$c_p = c_v + T\left(\frac{\partial p}{\partial T}\right)_\rho^2 \chi_T \tag{B2}$$

The isothermal compressibility coefficient χ_T and the specific heat at constant volume are given by the restricted cubic model [8]. For the reference hydrodynamic DNS we used a constant c_v value calculated for the initial value of temperature and density. We used a constant value for the viscosity μ: $3.74 \cdot 10^{-5}$ Pa·s for SF_6 and $3.45 \cdot 10^{-5}$ Pa·s for CO_2.

Appendix C

According to the integral theorem about the mean value [24], there is always a point $\vec{x}_m \in v$ so that

$$\int_v Y(\vec{x})Z(\vec{x})\mathrm{d}\vec{x} = Y(\vec{x}_m)\int_v Z(\vec{x})\mathrm{d}\vec{x} \tag{C1}$$

if the functions Y, Z are continuous. When the spatial variation of Y in v is small, $\langle Y\rangle \approx Y(\vec{x}_m)$ and Eq. 17 stems from Eq. (C1).

Appendix D: Application of the Finite Volume Method (FVM) and SIMPLER algorithm

According to the FVM, the calculation domain is divided into a number of non-overlapping control volumes so that there is one control volume surrounding each grid point. The differential equations are integrated over each control volume. The attractive feature of this method is that the integral balance of mass, momentum, and energy is exactly satisfied over any control volume (called below the cell for the sake of brevity), and thus over the whole calculation domain. The integral formulation is also more robust than the finite difference method for problems which present strong variations of properties observed in a near-critical fluid [10, 20]. The equations are resolved on a staggered grid. This means that the velocity is computed at the points that lie on the faces of the cell while the scalar variables (pressure, density and temperature) are computed at the center of the cell. This choice is made to avoid pressure oscillations in the computations [11]. For the time discretization, the first order Euler scheme is used. For the sake of simplicity and clarity we present the finite volume method for the 1D generalized transport equation for a variable Y (where Y can be substituted by either u or T)

$$\frac{\partial \rho Y}{\partial t} + \frac{\partial \rho u Y}{\partial x} = \frac{\partial}{\partial x}\left(\Gamma\frac{\partial Y}{\partial x}\right) + S \tag{D1}$$

where Γ denotes the generalized diffusion coefficient and S the generalized source term (volume forces). Integrated over the ith cell of the length δx, Eq. (D1) takes the form

$$\frac{\rho_P Y_P - \rho_P^p Y_P^p}{\Delta t}\Delta x + J_e - J_w = S_P \Delta x \tag{D2}$$

where the superscript p denotes the value on the previous time step, the subscript P represents the center of the cell, the subscripts e and w its "east" and "west" face respectively. The calculation of the flux

$$J = \rho u Y - \Gamma\frac{\partial Y}{\partial x} \tag{D3}$$

on the faces requires the knowledge of Y and ρ at the *centers* of two neighboring "East" and "West" cells denoted by the *capital* letters E and W. Their values at the faces can be found by linear interpolation between their values at the centers, e.g. $Y_e = 0.5(Y_P + Y_E)$ if the nodes are equidistant.

The continuity equation integrated on the control volume is given by:

$$\frac{\rho_P - \rho_P^p}{\Delta t}\Delta x + F_e - F_w = 0 \tag{D4}$$

with $F = \rho u$. When multiplying Eq. (D4) by Y_P and subtracting the result from Eq. (D2), one obtains the equation

$$\frac{\rho_P^p \Delta x}{\Delta t}(Y_P - Y_P^p) + (J_e - Y_P F_e) - (J_w - Y_P F_w) = S_P \Delta x \tag{D5}$$

that can be rewritten in the following form

$$a_P Y_P = a_W Y_W + a_E Y_E + b \tag{D6}$$

The tridiagonal set of linear equations (D6) with respect to Y_P is solved by the Thomas algorithm [25]. The stencil coefficients a_P, a_W et a_E depend on the discretization scheme. Their general expression is

$$\begin{array}{l} a_W = B_w A_w + \max(-F_w, 0), \\ a_E = B_e A_e + \max(F_e, 0), \\ a_P = a_W + a_E + \rho_P^p \Delta x/\Delta t, \\ b = S_P \Delta x + \rho_P^p Y_P^p \Delta x/\Delta t, \end{array} \tag{D7}$$

where $B = \Gamma/\Delta x$. We use the "power law scheme" [11] that requires

$$A_i = \max\left[0, \left(1 - \frac{0.1|F_i|}{B_i}\right)^5\right], \quad i = e, w.$$

The set (D6) should be written and solved both for the velocity and the temperature. While the above scheme can be directly applied for the temperature case, the coupling of the velocity and the pressure $p^{(1)}$ (which is defined implicitly by the continuity equation) requires a special treatment for the velocity equation as described below.

The non-dimensionalized and discretized Navier-Stokes equation (30)

$$a_e u_e = \sum a_{nb} u_{nb} + (p_P^{(1)} - p_E^{(1)}) + b, \tag{D8}$$

where the subscript nb denotes the neighbors of the point e, can be solved only when the pressure field is given. Unless the correct pressure field is employed, the resulting velocity field will not satisfy the continuity equation. We use the iterative SIMPLER algorithm [11] to couple the velocity and the pressure fields. This algorithm is based on successive corrections of the velocity field and pressure field at a given time step. The velocity and pressure variables are decomposed as follows:

$$\begin{array}{l} u = u^* + u', \\ p^{(1)} = p^{(1)*} + p^{(1)\prime}, \end{array} \tag{D9}$$

where the asterisk denotes the guesses and prime the corrections. The steps of the SIMPLER algorithm are the following:

1. Start with a guessed velocity field.

2. A pseudo-velocity $\widehat{u}$ (without taking into account the pressure gradient) is first computed and is defined as

$$\widehat{u}_e = \frac{\sum a_{nb} u_{nb} + b}{a_e} \tag{D10}$$

where u_{nb} represents the neighbor velocities. $\widehat{u}$ satisfies

$$u_e = \widehat{u}_e + \frac{p_P^{(1)*} - p_E^{(1)*}}{a_e}. \tag{D11}$$

3. Compute the pressure $p^{(1)*}$ whose equation is deduced by applying the divergence operator to Eq. (D11) and using the continuity equation (D4):

$$\left(\frac{\rho_w}{a_w} + \frac{\rho_e}{a_e}\right) p_P^{(1)*} = \frac{\rho_w}{a_w} p_W^{(1)*} + \frac{\rho_e}{a_e} p_E^{(1)*} + \frac{\rho_P^p - \rho_P}{\Delta t}\Delta x - \rho_e \widehat{u}_e + \rho_w \widehat{u}_w. \tag{D12}$$

4. Solve Eq. (D8) with $p^{(1)*}$ used for $p^{(1)}$ and thus obtaining u^*.

5. Compute $p^{(1)\prime}$ whose equation is obtained analogously to Eq. (D12) from

$$u_e = u_e^* + \frac{(p_P^{(1)\prime} - p_E^{(1)\prime})}{a_e}. \tag{D13}$$

It takes the form

$$\left(\frac{\rho_w}{a_w} + \frac{\rho_e}{a_e}\right) p_P^{(1)\prime} = \frac{\rho_w}{a_w} p_W^{(1)\prime} + \frac{\rho_e}{a_e} p_E^{(1)\prime} + \frac{\rho_P^p - \rho_P}{\Delta t}\Delta x - \rho_e u_e^* + \rho_w u_w^*. \tag{D14}$$

6. Calculate the velocity u using Eq. (D13). Do not correct the pressure $p^{(1)}$, $p^{(1)\prime}$ is used to correct only the velocity field, the pressure being computed by Eq. (D14).

7. Solve the energy equation for T using the obtained u values.

8. Calculate the density distribution and $p^{(0)}$ via Eqs. (33,34).

9. Return to step 2 and repeat until the converged solution is obtained.

It has to be noted that whereas the fractional step PISO algorithm [10] is successful in resolving the equations (29-32) on the acoustic time scale, it is not the case when the acoustic filtering method is used. Due to the different meanings of pressure (see the subsection III C) in the momentum equation (involving $p^{(1)}$) and in the energy equation (involving $p^{(0)}$), it appears that only an iterative algorithm can correctly couple the thermodynamic field and the velocity field, the PISO algorithm leading to unstable solutions.

[1] B. Zappoli, D. Bailly, Y. Garrabos, B. Le Neindre, P. Guenoun, & D. Beysens, Phys. Rev. A **41**, 2264 (1990).

[2] A. Onuki & R.A. Ferrell, Physica A **164**, 245 (1990).

[3] D. Beysens, D. Chatain, V. S. Nikolayev, & Y. Garrabos, *Magnetic facility gives heat transfer data in H2 at various acceleration levels*, 4th Int. Conf. on Launcher Technology "Space Launcher Liquid Propulsion", 3-6/12/2002, Liege, Belgium (2002).

[4] D. Beysens, D. Chatain, V.S. Nikolayev, Y. Garrabos, & A. Dejoan, *Fast heat transport under weightlessness*, to be published.

[5] H. Boukari, J.N. Shaumeyer, M.E. Briggs, & R.W. Gammon, Phys. Rev. A **41**, 2260 (1990).

[6] J. Straub, L. Eicher, & A. Haupt, Phys. Rev. E **51**, 5556 (1995).

[7] F. Zhong & H. Meyer, Phys. Rev. E **51**, 3223 (1995).

[8] M.R. Moldover, J.V. Sengers, R.W. Gammon, & R.J. Hocken, Rev. Mod. Phys. **51**, 79 (1979); note that χ_T is defined differently.

[9] B. Zappoli & P. Carlès, Eur. J. Mech. B/Fluids **14**, 41 (1995).

[10] S. Amiroudine, J. Ouazzani, P. Carlès & B. Zappoli, Eur. J. Mech. B/Fluids **16**, 665 (1997).

[11] S. V. Patankar *Numerical heat transfer and fluid flow*, Hemisphere, Washington (1980).

[12] Y. Garrabos, M. Bonetti, D. Beysens, F. Perrot, T. Fröhlich, P. Carlès & B. Zappoli, Phys. Rev. E **57** 5665 (1998).

[13] Y. Chiwata & A. Onuki, Phys. Rev. Lett. **87**, 144301 (2001).

[14] A. Furukawa & A. Onuki, Phys. Rev. E **66**, 016302 (2002).

[15] D. Bailly & B. Zappoli, Phys. Rev. E **62**, 2353 (2000).

[16] B. Zappoli, S. Amiroudine, P. Carlès & J. Ouzzani, J. Fluid Mech. **316**, 53 (1996).

[17] A. Jounet, Phys. Rev. E **65**, 037301 (2002).

[18] Y. Garrabos, A. Dejoan, C. Lecoutre, D. Beysens, V. Nikolayev & R. Wunenburger, J. Phys. (France) **11** Pr6-23 (2001).

[19] S. Paolucci, SAND 82-8257, Sandia National Laboratories, Livermore (1982).

[20] B. Zappoli & A. Durant-Daubin, Phys. Fluids **6**, 1929 (1994).

[21] C.A. Brebbia, J.C.F. Telles & L.C. Wrobel *Boundary Element Techniques*, Springer, Berlin (1984).

[22] V.S. Nikolayev, D.A. Beysens, G.-L. Lagier & J. Hegseth, Int. J. Heat Mass Transfer **44**, 3499 (2001).

[23] V.S. Nikolayev & D.A. Beysens, in: *Boundary Elements XXIV*, Int. Ser. Adv. Boundary Elements, v.13, Eds. C.A. Brebbia, A. Tadeu & V. Popov, WIT press, Southhampton, 511 (2002).

[24] G. Korn & T. Korn, *Mathematical handbook for scientists and engineers*, Dover, New York (2000).

[25] D.A. Anderson, J.C. Tannehill & R.H. Pletcher *Computational Fluid Mechanics* Hemisphere Publishing Corporation, New York (1984).

[26] D. Beysens, T. Fröhlich, V.S. Nikolayev, & Y. Garrabos, *Jets in near-critical fluid*, to be published.